Palestine Journal of Mathematics

Vol 15(1)(2026) , 93–107

EFFECT OF VARIABLE HEAT SOURCE AND VISCOSITY ON THE ONSET OF BÉNARD MAGNETOCONVECTION USING RAYLEIGH-RITZ TECHNIQUE: LINEAR STABILITY ANALYSIS

A. S. Aruna, Vijaya Kumar, K. R. Milana and N. Kavitha

Communicated by: Geeta Arora

MSC 2020 Classifications: Primary 76E06; Secondary 76R10.

Keywords and phrases: Rayleigh-Bénard magnetoconvection, Higher order Rayleigh Ritz method, Galerkin's expansion, Variable heat source, Linear theory.

The authors are grateful to senior Professor P. G. Siddheshwar, Christ University, Bangalore for his suggestion and also to the management and Principal, RIT, Bangalore for the support.

Corresponding Author: A. S. Aruna

Abstract. Rayleigh–Bénard convection plays an important role in many natural and engineering problems, such as geophysical convection, heat transfer in industrial systems, crystal growth, and cooling of electronic devices. Most earlier studies on Rayleigh–Bénard convection (RBC) with variable viscosity examine only a limited set of boundary conditions and usually do not include the effects of internal heat source/sink and magnetic field. Therefore, this study aims to analyze the effects of an internal heat source, variable viscosity, and an applied magnetic field on the onset of Rayleigh–Bénard convection by considering ten different boundary combinations, including free–free, rigid–free, and rigid–rigid cases with both isothermal and adiabatic thermal boundaries. To perform linear theory, the higher-order Rayleigh-Ritz method is employed, and the eigenvalue problem is solved. It is found that the three-term Galerkin expansion method is good enough to estimate the critical Rayleigh number and wave number. It is shown that as the Chandrasekhar number increases, the critical Rayleigh number and wave number increases, thereby stabilizing the system. But in case of increasing thermorheological parameter and internal Rayleigh number, the critical Rayleigh number and wave number decreases and destabilizes the same. Study also demonstrates, among all the ten boundary combinations, the most stable combination is LRI-URI, while the least one is LFA-UFA. These findings provide new insight into the coupled influence of magnetic fields, internal heating, and viscosity under diverse boundary constraints, extending and generalizing earlier RBC.

1 Introduction

Rayleigh–Bénard magnetoconvection refers to buoyancy-driven natural convection that occurs in the presence of a magnetic field. This phenomenon plays an important role in several areas such as astrophysics, geophysics, crystal growth, and disease detection. Early investigations by Chandrasekhar [1] and Danielson [2] showed that applying a magnetic field makes convection patterns more orderly and stable by suppressing turbulence in Rayleigh–Bénard convection. Later, Calkins et al. [3] reported the existence of different flow regimes, including two-dimensional and anisotropic three-dimensional structures, when a magnetic field is present. Bhattacharya et al. [4] examined the influence of inclined magnetic fields on the critical Rayleigh number and the size of convection cells, while Zürner et al. [5] demonstrated that vertical magnetic fields can significantly weaken large-scale circulation in liquid metals. McCormack et al. [6] further explored bifurcations and chaotic behavior in convection under vertical magnetic fields. More recently, Aruna [21] carried out a weakly nonlinear analysis of Rayleigh–Bénard magnetoconvection in a Newtonian fluid with variable viscosity and an internal heat source. The study

revealed that the magnetic field increases the critical Rayleigh number, thereby stabilizing the system and reducing heat transfer, a trend also observed by Ramachandramurthy and Aruna [22] and Kavitha et al. [23].

The Viscosity of liquid is closely related to internal friction, and many studies on convective instability have relied on the Boussinesq approximation, which assumes temperature-dependent viscosity. This phenomenon is known as the thermorheological effect. The investigation of convection in Newtonian liquids with variable viscosity has gained attention due to the thermorheological character of various fluids. However, many researchers have overlooked the impact of temperature-dependent viscosity in the Rayleigh-Bénard convection problem, despite its significant influence on system stability. For instance, both water and silicone oil exhibit considerable changes in kinematic viscosity with temperature variations. Booker [7] and Booker and Stengel [8] demonstrate how the critical Rayleigh number varies when viscosity changes with temperature, and affects the stability of the system. The effect of strong viscosity variation with temperature is illustrated by Torrance and Turcotte [9], considering the exponential model. Furthermore, Kassoy and Zebib [10], Busse and Frick [11], Nield [12], Siddheshwar [13] are all based on temperature-dependent viscosity and found that the thermorheological parameter enhances heat transfer. Pla and Henar [14] analyzed a convective solution for a two-dimensional fluid layer with viscosity exponentially dependent on temperature.

In most cases, the material provides its own heat source, which increases the pressure in the liquid. This can occur in various settings, including the presence of radioactivity and chemical reactions. This mechanism can also occur on some celestial objects because nuclear reactions and radioactivity make them active. Due to internal heat generation, a temperature gradient exists between the center of the Earth and its surface, which helps maintain the Earth's temperature, allowing thermal energy to be transferred to the Earth's surface (see Giannandrea and Christensen [15]). Tveitereid and Palm [16] and Clever [17] studied the effect of internal heat generation on the onset of Rayleigh-Bénard convection and showed that the heat source/sink can effectively be used to suppress or enhance convection. Further, Riahi et al. [18]-[19] performed an unsteady analysis of RBC with the effect of internal heat source/sink and found that the its effect is to advance the onset of convection. Recent studies: Siddheshwar and Titus [20], Aruna [21], Ramachandramurthy and Aruna [22], Kavitha et al. [23], Ramachandramurthy et al. [24] and Ogunmola et al. [25]) are based on variable heat source/sink. They derived generalized Lorenz model using Fourier series method and found that the heat transfer can be enhanced in the presence of heat source.

Recently, Siddheshwar et al. [31] made linear stability analysis Rayleigh-Bénard and Bénard-Marangoni convection with variable viscosity effect. They made detailed study on the impact of different boundary combination on the onset of stability (also see Gangadharaiah et al.[29], Arora and Sharma [30], Aravind and Ravikumar [31] and references their in). But the unconsidered aspect of the study is the effect of variable heat source/sink and exponentially varying viscosity. To the best of authors knowledge, the Rayleigh-Bénard magnetoconvection problem with variable viscosity and internal heat source/sink, across ten different boundary conditions, has not yet been explored. Therefore the current research examines the analytical study of RBC in the presence of variable heat source/sink along with magnetic field. This study contains an exponential viscosity model proposed by Torrance and Turcotte [9] (also see Aruna et al. [33], Amendola et al. [34], Akinshilo et al. [35] an Das et al. [36]). Higher order Rayleigh-Ritz method is employed to determine eigenvalues of the problem. Also, we assume the variation of thermal conductivity with temperature is negligible (Yutikas and Zhukauskas [26]).

2 Flow configuration and mathematical formulation

Consider an infinitely extended horizontal layer of electrically conducting Newtonian fluid of depth d that is heated from below and cooled above as shown in the Fig. 1 (maintain lower boundary temperature as $T_0 + \Delta T$ and upper boundary temperature as T_0). Here we considered the temperature-dependent variable viscosity as one of the important characteristic of the fluid

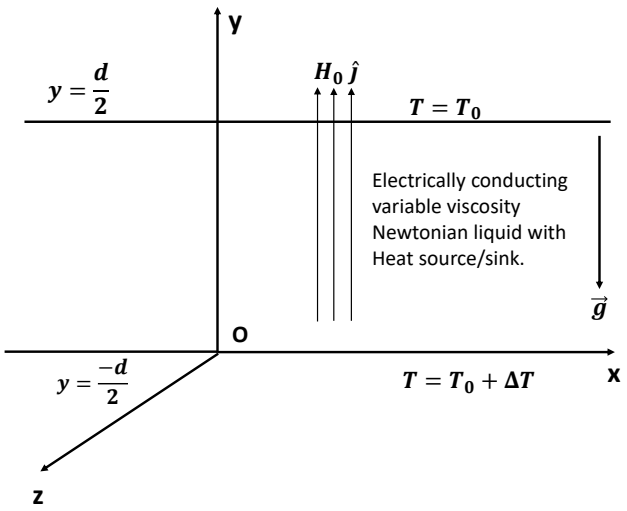

Figure 1. Schematic flow configuration:

with internal heat source/sink. A Cartesian coordinate system is considered with the origin positioned at the bottom of the fluid layer and the y-axis oriented vertically upwards. In this problem, the fluid is subjected to both a temperature gradient and a uniform magnetic field of magnitude H_0. The physical properties of the fluid, including dynamic viscosity, density, and internal heat generation, are considered to vary with temperature. The governing equations of the flow configuration describing this Rayleigh-Bénard situation are as follows:

Conservation of linear momentum:

$$\rho_0\left(\frac{\partial u_i}{\partial t}+u_j\frac{\partial u_i}{\partial x_j}\right)=-\frac{\partial p}{\partial x_i}+\rho g_i+\nabla.\left(\mu_f(T)\left(\frac{\partial u_i}{\partial x^i}+\frac{\partial u_j}{\partial x^i}\right)\right)-\mu_m^2\sigma H_0^2 u_i. \tag{2.1}$$

The Navier-Stokes momentum equation is supplemented by the following components equations:

Conservation of mass:

$$\frac{\partial u_i}{\partial x^i}=0. \tag{2.2}$$

Advection-diffusion equation:

$$\frac{\partial T}{\partial t}+u_i\frac{\partial T}{\partial x^j}=\kappa\frac{\partial^2 T}{\partial x_i^2}+H_s(T-T_0). \tag{2.3}$$

Density equation:

$$\rho(T)=\rho_0\left(1-\alpha(T-T_0)\right). \tag{2.4}$$

Temperature-dependent viscosity equation (Torrance and Turcotte (1971)):

$$\mu_f(T)=\mu_0 e^{-\delta(T-T_0)}. \tag{2.5}$$

Where $u_i=(u,v,w)$ is the fluid velocity in vector form, $\rho(T)$ is temperature-dependent density, p is the hydro static pressure, and $\mu_f(T)$ is temperature dependent viscosity, $g_i=(0,-g,0)$ is the gravitational constant, μ is magnetic permeability, H_0 is the uniform magnetic field applied in the y-direction , ρ_0 is the reference density at temperature T_0, κ is the thermal diffusivity of the conducting fluid, H_s is the temperature-dependent heat source/sink, $\alpha>0$ is the coefficient of thermal expansion and μ_0 is the reference viscosity. The Oberbeck-Boussinesq approximation

is difficult even for Navier-Stokes fluids. In practice, the density variation can occur only in the Buoyancy term. In addition to assuming a temperature-dependent viscosity and heat source, we also deal with a magnetohydrodynamics version of the classical Rayleigh-Bénard problem, the two factors of magnetic field and temperature-dependent viscosity influence the onset of convection. It is clear that they are antagonistic in their effects. With this assumption, we assumes that the Oberbeck-Boussinesq approximation is valid. The time-independent basic quiescent state solution (conduction state) of these equation are obtained as follows:

$$u_b = (0,0),\ \frac{dp_b}{dy} = -\rho_b g\hat{j},\ \rho_b = \rho_0\left(1 - \frac{\alpha\Delta T \sin\left(\sqrt{\frac{H_s d^2}{\kappa}}\left(\frac{1}{2} - \frac{y}{d}\right)\right)}{\sin\left(\sqrt{\frac{H_s d^2}{\kappa}}\right)}\right), \tag{2.6}$$

the basic temperature gradient for the present boundary conditions is given by

$$T_b - T_o = \Delta T\left(\frac{\sin\left(\sqrt{\frac{H_s d^2}{\kappa}}\left(\frac{1}{2} - \frac{y}{d}\right)\right)}{\sin\left(\sqrt{\frac{H_s d^2}{\kappa}}\right)}\right), \tag{2.7}$$

similarly, the basic viscosity as a function of y-axis is obtained to be

$$\mu_{fb}(y) = \frac{\mu_0 \sin\left(\sqrt{\frac{H_s d^2}{\kappa}}\right)}{\sin\left(\sqrt{\frac{H_s d^2}{\kappa}}\right) + \delta\Delta T \sin\left(\sqrt{\frac{H_s d^2}{\kappa}}\left(\frac{1}{2} - \frac{y}{d}\right)\right)}. \tag{2.8}$$

We now superimpose infinitesimal perturbations to the basic state. Using the classical approach to linear stability analysis, and choosing d as the characteristic length scale, $\frac{d^2}{\kappa}$ as the time scale, and βd as the temperature scale, the resulting dimensionless equations that describe small perturbations are given by:

$$\rho_0\frac{\partial u'_i}{\partial t} = -\frac{\partial p}{\partial x_i} - \rho' g\hat{j} + \frac{\partial \mu_{fb}}{\partial x_j}\left(\frac{\partial u'_i}{\partial x_j} + \frac{\partial u'_j}{\partial x_i}\right) + \mu_{fb}\frac{\partial^2 u'_i}{\partial x_j^2} - \mu_m^2\sigma H_b^2 u'_i, \tag{2.9}$$

$$\frac{\partial T'}{\partial t} + w'\frac{dT_b}{dy} = \kappa\frac{\partial^2 T'}{\partial x_i} + H_s T', \tag{2.10}$$

where $\rho' = -\alpha\rho_0 T'$ be the deviation of density from the basic state and the primes indicates the perturbed quantities. We shall now consider the x, y and z component of the Eqn. (2.9) and eliminate the pressure term by the classical procedure (Siddheshwar et al. [28]), then we obtain

$$\begin{array}{l}\rho_0\frac{\partial}{\partial t}(\nabla^2 w') = \alpha\rho_0 g\nabla_1^2 T' + \mu_{fb}\nabla^4 w' + 2\frac{\partial\mu_{fb}}{\partial y}\frac{\partial}{\partial z}\left(\nabla^2 w'\right) \\ +\frac{\partial^2\mu_{fb}}{\partial y^2}\left(\frac{\partial^2 w'}{\partial y^2} - \nabla_1^2 w'\right) - \mu_m^2\sigma H_b^2\nabla^2 w'.\end{array} \tag{2.11}$$

Non-dimensionalize Eqs. (2.10) and (2.11) using the following definitions (refer Siddheshwar and Stephen Titus [20]):

$$(x', y') = d(x^*, y^*),\ t = \frac{d^2}{\kappa}t^*,\ T' = \beta d T^*,\ w' = \frac{\kappa}{d}w^* \tag{2.12}$$

and we obtain the the following equations involving dimensionless parameters (after dropping asterisk)

$$\begin{array}{l}\frac{1}{\mathrm{Pr}}\frac{\partial}{\partial t}(\nabla^2 w) = R_E\nabla_1^2 T + \mu_{fb}\nabla^4 w + 2\frac{\partial\mu_{fb}}{\partial y}\frac{\partial}{\partial y}\left(\nabla^2 w\right) \\ +\frac{\partial^2\mu_{fb}}{\partial y^2}\left(\frac{\partial^2 w}{\partial y^2} - \nabla_1^2 w\right) - Q\nabla^2 w\end{array}, \tag{2.13}$$

$$\frac{\partial T}{\partial t} - \nabla^2 T = -w\frac{dT_b}{dy} + R_I T. \tag{2.14}$$

Where Pr $= \frac{\mu_0}{\kappa\rho_0}$ is the Prandtl number, $R_E = \frac{\alpha\beta g d^4 \rho_0}{\mu_0 \kappa}$ is the thermal Rayleigh number and it is the eigenvalue of the problem, $Q = \frac{\mu_m^2 \sigma H_0^2 d^2}{\mu_0}$ is the Chandrasekhar number, $V = \delta\Delta T$ be the thermorheological parameter, and $R_I = \frac{H_s d^2}{\kappa}$ be the internal Rayleigh number. It is clear from the vertical component of momentum equation that the term $\frac{\partial^2 \mu_{fb}}{\partial y^2}\left(\frac{\partial^2 w}{\partial y^2} - \nabla_1^2 w\right)$ disappear when viscosity is linear function of temperature difference (see Severin and Herwig [27]). Most of the time viscosity-temperature relation is non-linear. In literature we find many such viscosity models. For example, an exponential model suggested by Torrence and Turcotte [9](also see Aruna and Kavitha [33]), quadratic model by Siddheshwar et al. [13]) and Neilds model by Neild [12]). These models are designed for different viscous fluid and explores the impact of variable viscosity on the stability of system. It is also clear from the energy Eqn. (2.14), when the internal Rayleigh number R_I is absent, the resultant equation turn out be the one reported by Siddheshwar et al. [28]. The principle of exchange of stability (PES) for fluids with constant viscosity hold, as discussed in Chandrasekhar [1]. In the case of fluids with variable viscosity, PES is assumed to be valid as discussed in Torrance and Turcotte [9]. Given the validity of PES, the solutions to Eqs. [2.13-2.14] can be represented as periodic waves, expressed in the form of normal mode solutions:

$$\left.\begin{array}{l} w(x,y,z) = w(z)e^{i(lx+my)} \\ T(x,y,z) = T(z)e^{i(lx+my)} \end{array}\right\}, \tag{2.15}$$

where l and m are the horizontal and vertical component of wave number and $\alpha = \sqrt{l^2+m^2}$ is the effective wave number. $w(z)$ and $T(z)$ are respectively the amplitudes of stream function and temperature distribution. Let us now substitute Eqn. [2.15] into Eqs. [2.13] and [2.14] and perform a normal mode analysis, which gives us a set of ordinary differential equations as follows:

$$\begin{array}{l} F(y)\left(D^2-k^2\right)^2 w + 2VF^2(y)\left(D^2-k^2\right)Dw + 2V^2F^3(y)\left(D^2+k^2\right)w \\ -Q\left(D^2-k^2\right)w - R_E k^2 T = 0, \end{array} \tag{2.16}$$

$$\left(D^2-k^2\right)T - R_I T + G(y)w = 0, \tag{2.17}$$

Where D denotes the non-dimensional derivative operator $\dfrac{d}{dy}$, $F(y) = \frac{\sin\sqrt{R_I}}{\sin\sqrt{R_I}+V\sin(\sqrt{R_I}(0.5-y))}$ represents non-dimensional form of viscosity variation $\mu_{fb}(y)$ and $G(y) = \frac{-\sqrt{R_I}\cos(\sqrt{R_I}(0.5-y))}{\sin\sqrt{R_I}}$ is non-dimensional form of temperature gradient $\frac{dT_b}{dy}$ across the fluid layer.

In this study, we examine ten distinct boundary combinations to carry out the linear stability analysis. The boundary conditions along with their associated trial functions are adopted from Siddheshwar et al. [28]. Table 1 summarizes the various boundary conditions and the corresponding trial functions used for Rayleigh-Bénard magnetoconvection. The selection of trial functions w and T is determined by both the order of the differential equations governing w and T, as well as the imposed boundary conditions. The trial functions used in the Rayleigh–Ritz formulation are selected so that they satisfy the tabulated boundary conditions for each rigid/free and isothermal/adiabatic boundary combination listed in Table 1. Polynomial functions are widely used in Rayleigh–Bénard convection studies because they are smooth, mutually independent, and easy to handle within the Galerkin method. Most importantly, they can be constructed to meet the imposed velocity and temperature boundary conditions without approximation. In cases involving adiabatic thermal boundaries, trigonometric trial functions are employed since they naturally satisfy the zero heat-flux condition and provide an efficient representation of the temperature field.

3 Solution of eigenvalue problem using higher order Rayleigh-Ritz technique

In order to perform linear stability analysis, it is important to determine the eigenvalue, the thermal Rayleigh number of the problem. To obtain accurate value of R_E, we use three-term

Table 1. Boundary conditions and corresponding trial functions for the onset of Rayleigh-Bénard convection:

Case	Boundary combinations	Boundary conditions	Trial function
1.	Lower rigid isothermal (LRI)	$w = Dw = T = 0$ at $y = -1/2$	$w_1 = 16y^4 - 8y^2 + 1$
	Upper rigid isothermal (URI)	$w = Dw = T = 0$ at $y = 1/2$	$T_1 = 4y^2 - 1$
2.	Lower rigid adiabatic (LRA)	$w = Dw = DT = 0$ at $y = -1/2$	$w_1 = 16y^4 - 8y^2 + 1$
	Upper rigid isothermal(URI)	$w = Dw = T = 0$ at $y = 1/2$	$T_1 = 4y^2 + 4y - 3$
3.	Lower rigid isothermal (LRI)	$w = Dw = T = 0$ at $y = -1/2$	$w_1 = 8y^4 - 4y^3 - 6y^2 + y + 1$
	Upper free isothermal(UFI)	$w = D^2w = T = 0$ at $y = 1/2$	$T_1 = 4y^2 - 1$
4.	Lower rigid adiabatic (LRA)	$w = Dw = DT = 0$ at $y = -1/2$	$w_1 = 8y^4 - 4y^3 - 6y^2 + y + 1$
	Upper free isothermal(UFI)	$w = D^2w = T = 0$ at $y = 1/2$	$T_1 = 4y^2 + 4y - 3$
5.	Lower rigid adiabatic (LRA)	$w = D^2w = T = 0$ at $y = -1/2$	$w_1 = 16y^4 - 8y^2 + 1$
	Upper rigid adiabatic (URA)	$w = D^2w = T = 0$ at $y = 1/2$	$T_1 = \cos\left[\pi\left(y + \frac{1}{2}\right)\right]$
6.	Lower rigid isothermal (LRI)	$w = Dw = T = 0$ at $y = -1/2$	$w_1 = 8y^4 - 4y^3 - 6y^2 + y + 1$
	Upper free adiabatic (UFA)	$w = D^2w = DT = 0$ at $y = 1/2$	$T_1 = 4y^2 - 4y - 3$
7.	Lower free isothermal (LFI)	$w = D^2w = T = 0$ at $y = -1/2$	$w_1 = 16y^4 - 24y^2 + 5$
	Upper free isothermal (UFI)	$w = D^2w = T = 0$ at $y = 1/2$	$T_1 = 4y^2 - 1$
8.	Lower free adiabatic (LFA)	$w = D^2w = DT = 0$ at $y = -1/2$	$w_1 = 16y^4 - 24y^2 + 5$
	Upper free isothermal (UFI)	$w = D^2w = T = 0$ at $y = 1/2$	$T_1 = 4y^2 + 4y - 3$
9.	Lower rigid adiabatic (LRA)	$w = D^2w = DT = 0$ at $y = -1/2$	$w_1 = 8y^4 - 4y^3 - 6y^2 + y + 1$
	Upper free adiabatic (UFA)	$w = D^2w = DT = 0$ at $y = 1/2$	$T_1 = \cos\left[\pi\left(y + \frac{1}{2}\right)\right]$
10.	Lower free adiabatic (LFA)	$w = D^2w = DT = 0$ at $y = -1/2$	$w_1 = 16y^4 - 24y^2 + 5$
	Upper free adiabatic (UFA)	$w = D^2w = DT = 0$ at $y = 1/2$	$T_1 = \cos\left[\pi\left(y + \frac{1}{2}\right)\right]$

Rayleigh-Ritz technique. At this stage, we expand $w(y)$ and $T(y)$ in a series of trial functions as described below:

$$w(y) = \sum_{i=1}^{n} \alpha_i w_i(y), \tag{3.1}$$

$$T(y) = \sum_{i=1}^{n} \beta_i T_i(y), \tag{3.2}$$

where α_i and β_i are constants. Applying Rayleigh-Ritz technique, substituting Eqs. (3.1) and (3.2) into the linearized forms of Eqs. (2.16) and (2.17), and then integrating with respect to y over the interval $\left[-\frac{1}{2}, \frac{1}{2}\right]$, results in a system of homogeneous equations involving the systems governing parameters

$$A_{ij}\alpha_i + B_{ij}\beta_i = 0, \tag{3.3}$$

$$C_{ij}\alpha_i + D_{ij}\beta_i = 0. \tag{3.4}$$

where,

$$\begin{aligned} A_{ij} = &\left\langle w_j F(y) D^4 w_i \right\rangle - 2k^2 \left\langle w_j F(y) D^2 w_i \right\rangle + k^4 \left\langle w_j F(y) w_i \right\rangle \\ &+2\left\langle w_j G(y) D^3 w_i \right\rangle - 2k^2 \left\langle w_j G(y) D w_i \right\rangle + \left\langle w_j \tfrac{dG}{dy} D^2 w_i \right\rangle \quad , \\ &+k^2 \left\langle w_j \tfrac{dG}{dy} w_i \right\rangle - Q\left\langle w_j D^2 w_i \right\rangle + Qk^2 \left\langle w_j w_i \right\rangle \end{aligned}$$

$$B_{ij} = -R_E k^2 \left\langle T_j w_i \right\rangle,$$

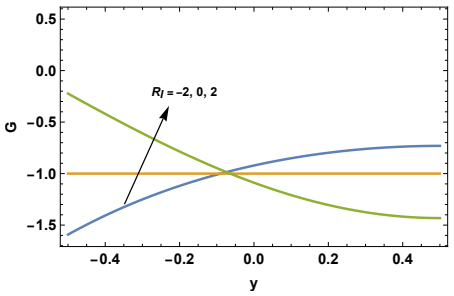

Figure 2. Basic temperature gradient plots for the different value of R_I:

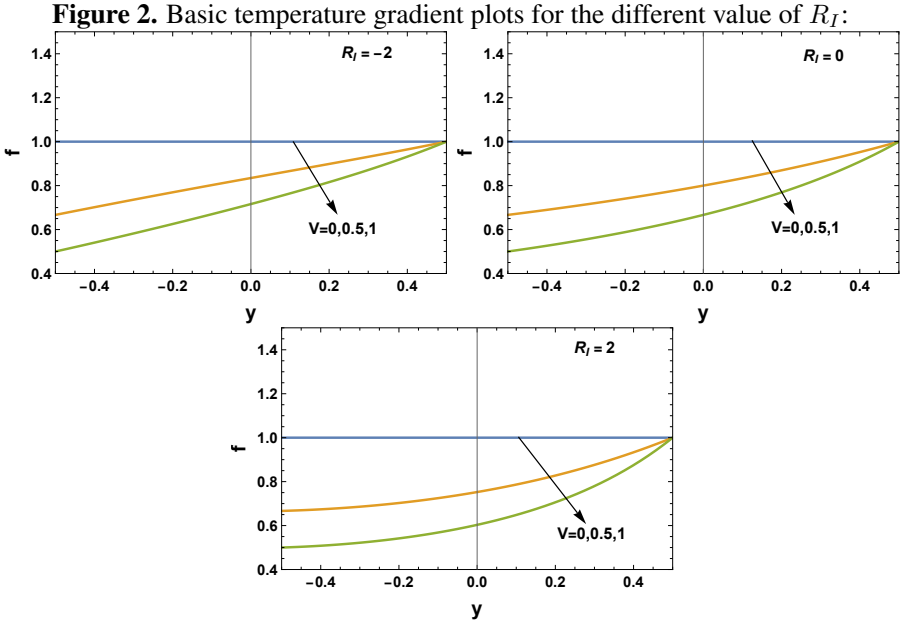

Figure 3. Basic viscosity variations plots over the depth of the fluid layer for the different values of V and R_I:

$$C_{ij} = -\langle w_j G(y) T_i \rangle ,$$
$$D_{ij} = \langle T_j D^2 T_i \rangle - k^2 \langle T_j T_i \rangle + R_I \langle T_j T_i \rangle .$$

Here the notation $\langle uv \rangle = \int_{-1/2}^{1/2} uv dy$. The homogeneous algebraic Eqs. (3.3) and (3.4) are essentially approximations to the dynamics of Rayleigh-Bénard system representing Eqs. (2.1)-(2.5). They are expressed in terms of α_i and β_i. Based on the boundary combinations detailed in Table 1, a set of trial functions for velocity and temperature are chosen and substituted into Eqs. (20) and (21). This process allows for the evaluation of the integrals that define the coefficients A_{ji}, B_{ji}, C_{ji}, and D_{ji}. For Eqs. (3.3) and (3.4) to admit a non-trivial solution, the determinant of the resulting coefficient matrix must vanish. This condition leads to a characteristic relationship among the parameters R_E, V, Q, and R_I, expressed as follows:

$$\Phi(R_E, R_I, V, Q, \alpha) = 0. \tag{3.5}$$

4 Results and discussion

The present study examines the effects of exponentially decreasing shear viscosity (Torrance and Turcotte [9], Ramachandramurthy and Aruna [22], and Aruna and Kavith [33]), the internal heat source/sink and the applied magnetic field on the onset of Rayleigh–Bénard convection by

considering ten different boundary combinations. The trial functions are derived based on the specific boundary combinations considered in the study. Thermorheological parameter typically include coefficients that describe how viscosity, shear stress and other rheological properties change with temperature. The Chandrasekhar number quantifies the balance between magnetic forces and viscous forces within the fluid. Higher the Chandrasekhar number indicates a stronger impact of the magnetic field, which can dampen convection currents and alter the flow patterns. The heat source/sink set up the temperature gradient across fluid layer and this significantly impact on convection. The efficiency and intensity of convection depends on the magnitude of the fluid such as its thermal conductivity, viscosity and temperature difference between the heat source/sink which often quantities by Rayleigh number.

In this study we have adopted three-term Rayleigh-Ritz technique to estimate the eigenvalues. The choice of a three-term Galerkin expansion is based on convergence. At the onset of convection, the system dynamics are dominated by the lowest eigenmodes, while higher-order modes have only a minor influence on the stability parameters. To verify this, convergence checks were carried out by increasing the number of Galerkin terms, and it was found that the critical Rayleigh number changes only marginally beyond three terms. This observation is consistent with earlier Rayleigh–Bénard convection studies, where similar low-order truncation have been shown to yield accurate and reliable results. Consequently, a three-term Galerkin expansion is good enough to estimate the eigenvalue of the problem.

Fig.(2) illustrate the variation of temperature gradient across the fluid layer for the different values of R_I. It is evident that when $R_I = 0$ the temperature gradient is linear function of y. Therefore, in the absence of heat source/sink the temperature variation across the fluid layer is linear in the basic conduction state. When $R_I = 2$ or $R_I = -2$, in the presence of heat source or sink, it is found that the temperature distribution is non-linear and become sinusoidal. However, these two plots are not symmetric and therefore these effects cannot be exactly opposite. Because, the internal heat source actively enhances buoyancy by creating unstable thermal gradient across the fluid layer, internal heat sink can only suppress instability within limits imposed by boundary conditions and thermal diffusion. Moreover, internal heating significantly alters the curvature of the basic temperature profile, whereas cooling primarily flattens it without producing a mirror image distribution.

Fig.(3) illustrate the variation of basic viscosity (in conduction state) over the depth of fluid layer, It is evident that the viscosity decreases from $e^{-V[\frac{1}{2}-z]}$ at the lower plate positioned at $z = -\frac{1}{2}$ but approaches 1 at the upper plate at $z = \frac{1}{2}$. Also it is evident that at $z = \frac{1}{2}$, the viscosity consistently equals to 1, regardless of the variations in the thermorheological parameter V and internal Rayleigh number R_I. These plots clearly shows that the viscosity which is temperature-dependent primarily affects the lower boundary, leading to earlier instability in the system compared to when viscosity remains constant.

Figs. (4) are the plots of Rayleigh number R_E versus wave number α for different values of Q for all ten boundary combinations given in Table 1. One can explicitly obtain R_E as the function of α, Q and V using single term Rayleigh Ritz method. But it is quite cumbersome for higher order. It is observed from all these plots that the effect of increasing Chandrasekhar number is to increase the critical Rayleigh number. Therefore, its effect is to stabilize the system for all boundary combination. This behavior can be attributed to the applied magnetic field, which imparts a degree of rigidity to the electrically conducting fluid, thus delaying the onset of convection. It is also observed that, as the Chandrasekhar number increases, the critical wave number also increases, indicating a shift of the instability towards shorter-wavelength convection cells. Physically, the magnetic field suppresses large-scale fluid motion by inducing Lorentz forces that oppose the velocity of the fluid in an electrically conducting fluid. Therefore, the magnetic field introduces stabilizing mechanism that resists the growth of thermal disturbances, thereby delaying the onset of convection.

The effect of internal Rayleigh number, R_I and the thermorheological parameter, V on critical Rayleigh and wave number is also depicted in the Fig. (4), these two parameter work together to destabilize the system and hence we find the antagonistic effect on the influence of magnetic

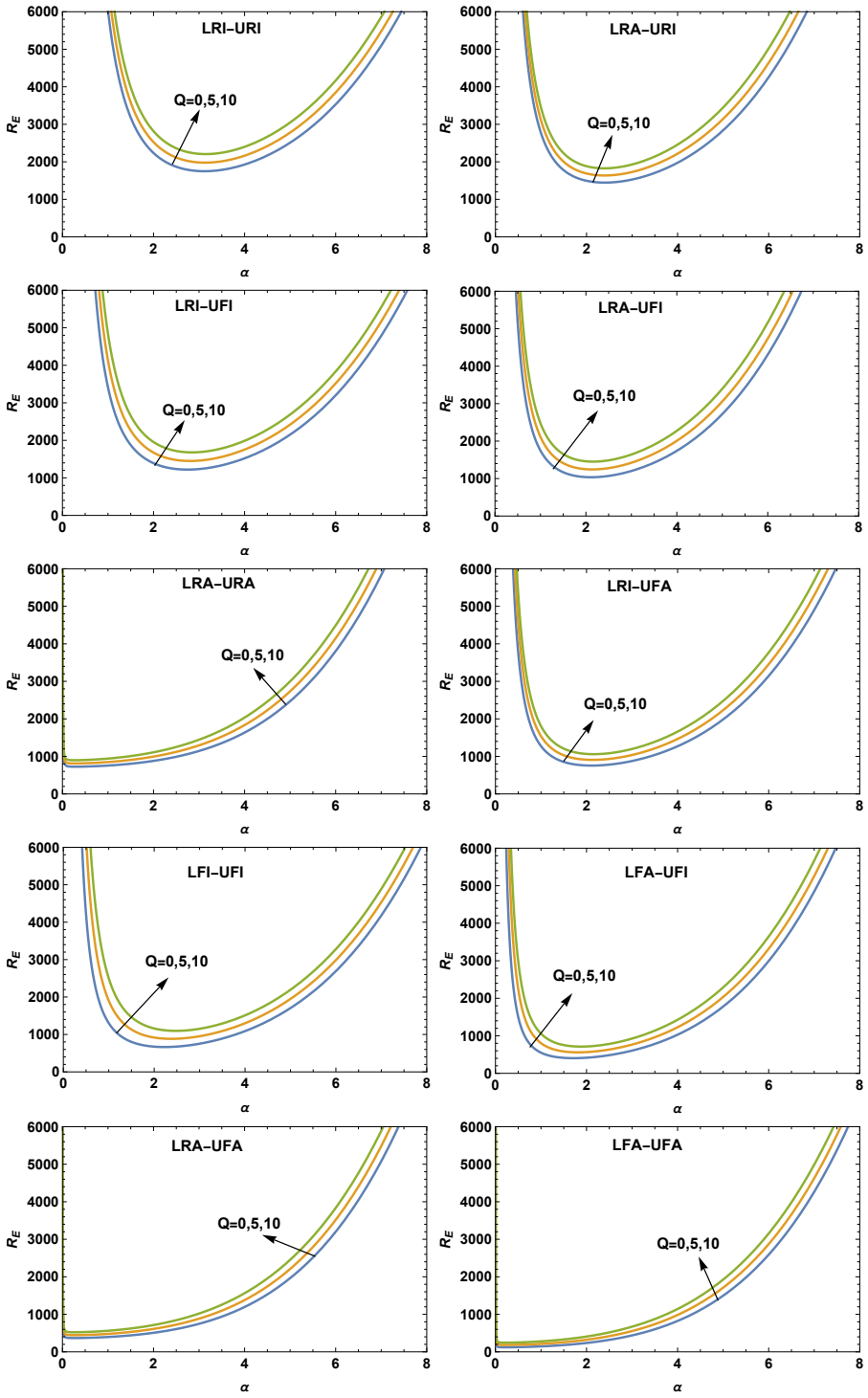

Figure 4. Plots of linear stability analysis curves-Neutral stability curves for different boundary conditions($V = 0, R_I = 0$):

Table 2. Critical values of the Rayleigh number R_{E_c} and the corresponding wave number α_c obtained using single term Rayleigh–Ritz techniques (RRT), when the internal Rayleigh number $R_I = -2$.

Boundary	$Q=0, V=0$		$Q=10, V=0$		$Q=0, V=1$		$Q=10, V=1$	
combination	R_{Ec}	α_c	R_{Ec}	α_c	R_{Ec}	α_c	R_{Ec}	α_c
LRI-URI	2032.180	3.214	2560.230	3.250	1487.990	3.221	2015.780	3.266
LRA-URI	1780.270	2.695	2249.350	2.697	1304.600	2.698	1773.680	2.701
LRI-UFI	1380.660	2.753	1933.590	2.882	1017.840	2.680	1574.160	2.862
LRA-UFI	1254.650	2.308	1791.600	2.390	912.408	2.204	1452.050	2.362
LRA-URA	1358.890	2.292	1715.320	2.278	996.211	2.294	1352.630	2.275
LRI-UFA	1004.360	2.308	1434.190	2.389	730.390	2.240	1162.380	2.362
LFI-UFI	789.333	2.294	1290.690	2.560	577.771	2.286	1075.510	2.617
LFA-UFI	533.548	1.929	915.390	2.125	389.767	1.920	770.008	2.163
LRA-UFA	758.041	1.959	1095.500	2.014	544.737	1.898	883.481	1.985
LFA-UFA	350.602	1.638	624.345	1.790	255.558	1.628	528.601	1.818

Table 3. Critical values of the Rayleigh number R_{E_c} and the corresponding wave number α_c obtained using single term Rayleigh–Ritz techniques (RRT), when the internal Rayleigh number $R_I = 0$.

Boundary	$Q=0, V=0$		$Q=10, V=0$		$Q=0, V=1$		$Q=10, V=1$	
combination	R_{Ec}	α_c	R_{Ec}	α_c	R_{Ec}	α_c	R_{Ec}	α_c
LRI-URI	1749.970	3.117	2206.720	3.145	1238.940	3.131	1695.410	3.166
LRA-URI	1446.390	2.399	1826.680	2.389	1026.320	2.405	1406.620	2.389
LRI-UFI	1138.700	2.670	1601.030	2.789	809.284	2.591	1274.550	2.767
LRA-UFI	947.438	2.052	1365.250	2.113	658.356	1.980	1078.190	2.081
LRA-URA	725.402	0.280	898.581	0.271	514.602	0.279	687.774	0.268
LRI-UFA	691.251	2.052	996.089	2.113	480.337	1.980	786.649	2.081
LFI-UFI	664.524	2.227	1096.290	2.478	469.525	2.204	898.983	2.532
LFA-UFI	404.135	1.716	712.659	1.880	283.119	1.691	591.273	1.905
LRA-UFA	323.405	0.236	477.343	0.237	211.865	0.224	365.811	0.230
LFA-UFA	121.861	0.195	244.665	0.210	82.640	0.191	205.449	0.210

Table 4. Critical values of the Rayleigh number R_{E_c} and the corresponding wave number α_c obtained using single term Rayleigh–Ritz techniques (RRT), when the internal Rayleigh number $R_I = 2$.

Boundary	$Q=0, V=0$		$Q=10, V=0$		$Q=0, V=1$		$Q=10, V=1$	
combination	R_{Ec}	α_c	R_{Ec}	α_c	R_{Ec}	α_c	R_{Ec}	α_c
LRI-URI	1482.220	2.998	1870.740	3.018	1001.400	3.022	1389.690	3.045
LRA-URI	1030.630	1.699	1294.220	1.670	699.575	1.699	963.093	1.661
LRI-UFI	909.691	2.568	1285.000	2.675	613.722	2.480	991.615	2.651
LRA-UFI	586.906	1.445	858.517	1.472	375.610	1.373	648.092	1.433
LRA-URA	476.321	0.000	754.239	0.000	268.715	0.000	589.641	0.000
LRI-UFA	378.216	1.445	553.248	1.472	242.052	1.373	417.645	1.433
LFI-UFI	546.366	2.144	911.31	2.379	366.384	2.100	730.573	2.426
LFA-UFI	240.113	1.205	449.788	1.307	155.317	1.164	365.444	1.311
LRA-UFA	168.910	0.000	389.641	0.000	108.329	0.000	278.641	0.000
LFA-UFA	96.631	0.000	278.491	0.000	89.137	0.000	169.352	0.000

field. An increase in R_I intensifies the volumetric heat generation within the fluid layer, thereby enhancing buoyancy forces and promoting thermal instability. Consequently, convection sets in at lower external Rayleigh number, leading to destabilization. Similarly, an increase in V reduces

Table 5. Critical values of the Rayleigh number R_{E_c} and the corresponding wave number α_c in the absence of magnetic field, variable viscosity and internal heat source or sink ($Q = V = R_I = 0$) obtained using two, three, and four-term Rayleigh–Ritz techniques (RRT), and compared with results from earlier studies.

Boundary	Second order RRT		Third order RRT		Fourth order RRT		Platten and Legros (1984)	
2-9 combination	R_{Ec}	α_c	R_{Ec}	α_c	R_{Ec}	α_c	R_{Ec}	α_c
LRI-URI	1750.410	3.110	1708.412	3.110	1706.751	3.116	1707.762	3.12
LRA-URI	1320.789	2.540	1304.490	2.543	1303.462	2.561	1295.781	2.55
LRI-UFI	1151.010	2.691	1112.020	2.672	1112.020	2.670	1100.657	2.680
LRA-UFI	885.400	2.220	816.864	2.241	816.777	2.214	816.748	2.210
LRA-URA	725.493	0.282	720.142	0.023	720.142	0.023	720.000	0.000
LRI-UFA	672.400	2.020	669.001	2.049	669.001	2.048	669.001	2.050
LFI-UFI	664.525	2.227	656.998	2.222	657.593	2.221	657.511	2.220
LFA-UFI	393.300	1.730	389.665	1.777	387.558	1.758	384.693	1.760
LRA-UFA	330.001	0.201	321.000	0.120	320.000	0.000	320.000	0.000
LFA-UFA	121.110	0.110	120.001	0.010	120.000	0.000	120.000	0.000

the dynamic viscosity in the fluid. This viscosity variation facilitating the growth of convective disturbances. As a result, thermal convection is further destabilized. Thus, the destabilizing effects of R_I and V counteract the stabilizing influence of the magnetic field.

Figs. (5)-(10) illustrate the graphs of R_{Ec} versus V, R_{Ec} versus Q, R_{Ec} versus R_I, α_c versus V, α_c versus Q and α_c versus R_I across different boundaries. These graphs encompass all ten boundary combinations considered in the study. It is evident from these plots that both R_Ec and α_c vary linearly with the parameters V, Q, R_I. Also, this trend is consistent across all boundary combinations is clearly seen in Table (2), (3) and (4). From these plots the following statements are evident

$R_{Ec}(LRI-URI) > R_{Ec}(LRA-URI) > R_{Ec}(LRI-UFI) >$
$R_{Ec}(LRA-UFI) > R_{Ec}(LRA-URA) > R_{Ec}(LRI-UFA) >$
$R_{Ec}(LFI-UFI) > R_{Ec}(LFA-UFI) > R_{Ec}(LRA-UFA) >$
$R_{Ec}(LFA-UFA)$

and

$\alpha_c(LRI-URI) > \alpha_c(LRI-UFI) > \alpha_c(LRA-URI) >$
$\alpha_c(LFI-UFI) > \alpha_c(LRA-UFI) > \alpha_c(LRI-UFA) >$
$\alpha_c(LFA-UFI) > \alpha_c(LRA-URA) > \alpha_c(LRA-UFA) >$
$\alpha_c(LFA-UFA)$

In particular, rigid–isothermal boundaries are more stabilizing than free–adiabatic boundaries because the no-slip condition at rigid walls suppresses velocity perturbations through increased viscous dissipation, while fixed-temperature (isothermal) boundaries efficiently damp thermal fluctuations. In contrast, free (stress-free) boundaries permit greater fluid motion with reduced viscous resistance, and adiabatic boundaries retain temperature perturbations within the fluid layer, thereby sustaining buoyancy forces. Consequently, convection sets in at higher critical Rayleigh numbers for rigid–isothermal boundary combination, indicating greater stability compared to free–adiabatic boundary conditions. The same trend is almost consistent across the parameters variation.

Table 5 compares the critical Rayleigh number R_{Ec} and the critical wave number α_c obtained using single-, two-, three-, and four-term Rayleigh–Ritz techniques with the existing literature. It is evident from the table that the change in both the critical Rayleigh number and the wave number from the third- to the fourth-order Rayleigh–Ritz technique is almost negligible, of the order of 10^{-3}. Therefore, a three-term Galerkin expansion is sufficient to accurately estimate the eigenvalues of the problem. Also, the critical Rayleigh number and the wave number obtained using the three-term Rayleigh-Ritz technique is in excellent agreement with Platten and Legros [36] and Siddheshwar et al. [28].

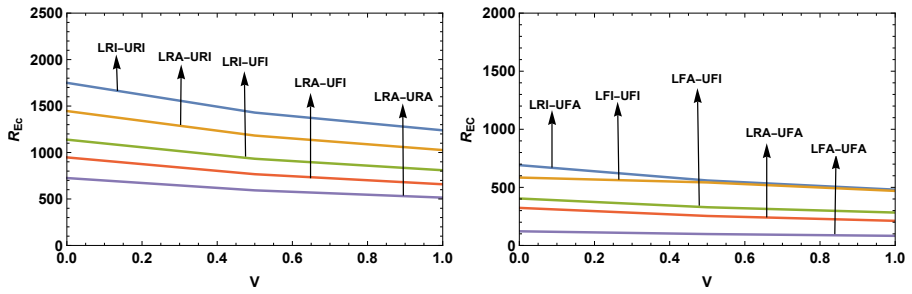

Figure 5. Plots R_{Ec} versus V for different boundary conditions when $Q = 0$,$R_I = 0$

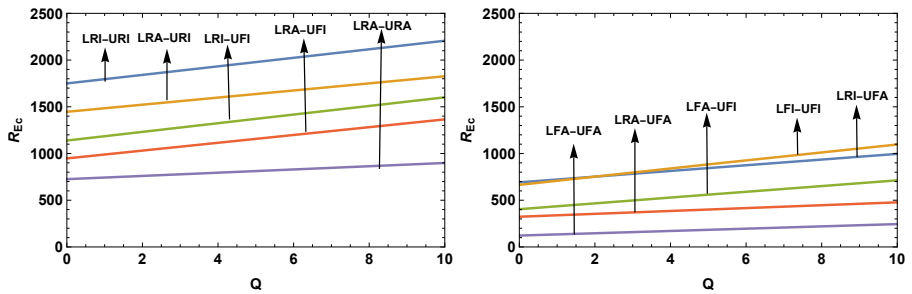

Figure 6. Plots R_{Ec} versus Q for different boundary conditions when $V = 0$,$R_I = 0$)

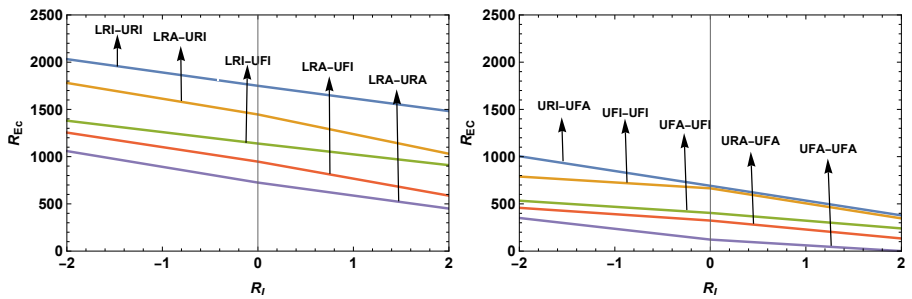

Figure 7. Plots R_{Ec} versus R_I for different boundary conditions when $V = 0$,$Q = 0$)

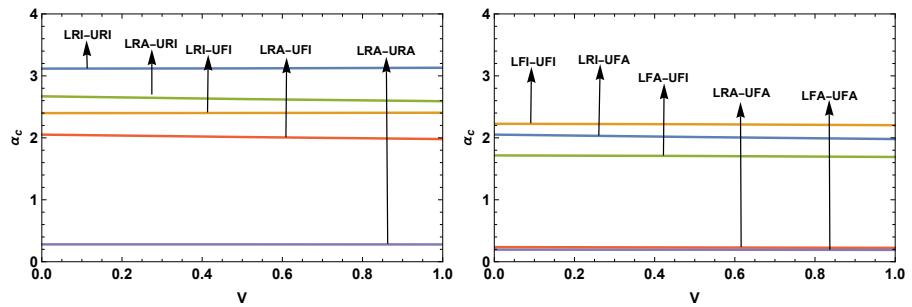

Figure 8. Plots α_c versus V for different boundary conditions when $Q = 0$,$R_I = 0$

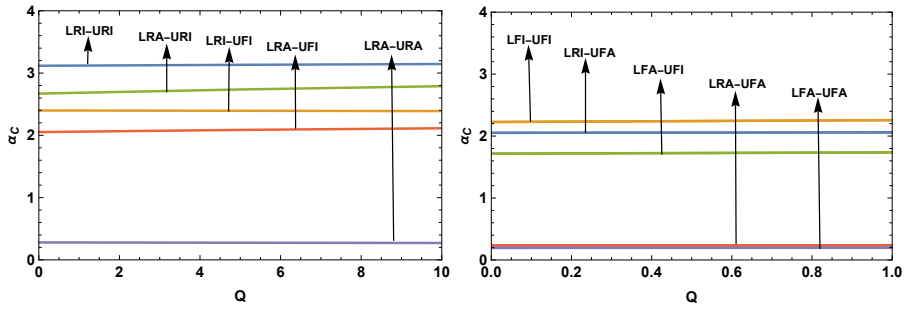

Figure 9. Plots α_c versus Q for different boundary conditions when $V = 0$,$R_I = 0$

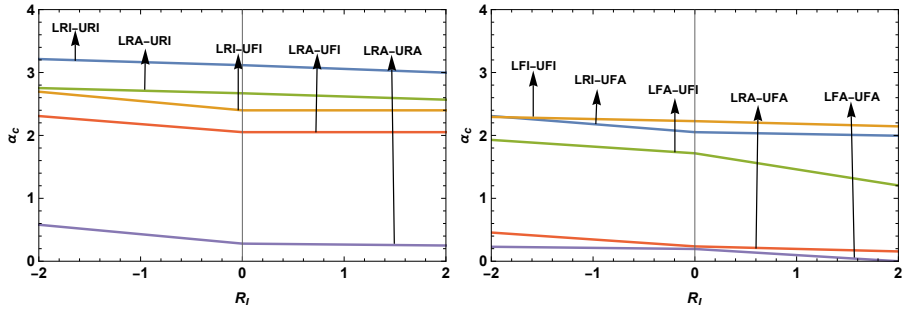

Figure 10. Plots α_c versus R_I for different boundary conditions when $V = 0$,$Q = 0$

5 Conclusions

This study explores how exponentially decreasing viscosity and internal heat source/sink affects the onset of Rayleigh-Bénard magneto-convection in an electrically conducting fluid, utilizing the specified ten boundary combinations given in Table 1. This study demonstrates that higher Order Rayleigh-Ritz method is effective for estimating the eigenvalues of the problem. In this study, however, a three-term Galerkin expansion is utilized to achieve the same. This study also demonstrates upon increasing the thermorheological parameter V, the critical Rayleigh number R_{Ec} decreases for all the ten boundary combinations. Therefore, its effect is to destabilize the system. The effect of increasing the Chandrasekhar number Q is to increase R_{Ec} and α_c, therefore the effect of magnetic field delay convection. Upon increasing the internal Rayleigh number R_I, R_{Ec} decreases, therefore, its effect is to destabilize the system. Among all the ten boundary combinations considered, the most stable combination is found to be LRI-URI, while the least stable combination is LFA-UFA. We conclude that these parameters can be effectively used either to enhance or delay the onset of convection.

References

[1] S. Chandrasekhar, *Hydrodynamic and Hydromagnetic Stability*, Courier Corporation, New York, (2013).

[2] R. E. Danielson, The structure of sunspot penumbras. II. Theoretical, *Astrophys. J.*, **134**, 289–304, (1961).

[3] M. A. Calkins, H. E. Huppert and G. Ahlers, Magnetoconvection in Rayleigh-Bénard cells: Quasistatic regimes and heat transport, *Phys. Fluids*, **35**, 104101, (2023).

[4] S. Bhattacharya, R. Subramanian and P. Mohanty, Wall-modes in Rayleigh-Bénard convection under inclined magnetic fields, *J. Fluid Mech.*, **877**, 564–593, (2023).

[5] M. Zürner, A. Fauchille and S. Wuest, Magnetic field effects on liquid metal Rayleigh-Bénard convection, *Phys. Rev. Fluids*, **5**, 043502, (2020).

[6] M. McCormack, H. L. Swinney and P. D. Weidman, Bifurcations and chaos in Rayleigh-Bénard convection under vertical magnetic fields, *Phys. Rev. Lett.*, **130**, 124503, (2023).

[7] J. R. Booker, Thermal convection with strongly temperature-dependent viscosity, *J. Fluid Mech.*, **76**, 741–754, (1976).

[8] J. R. Booker and K. C. Stengel, Further thoughts on convective heat transport in a variable-viscosity fluid, *J. Fluid Mech.*, **86**, 289–291, (1978).

[9] K. E. Torrance and D. L. Turcotte, Thermal convection with large viscosity variations, *J. Fluid Mech.*, **47**, 113–125, (1971).

[10] D. R. Kassoy and A. Zebib, Variable viscosity effects on the onset of convection in porous media, *Phys. Fluids*, **18**, 1649–1651, (1975).

[11] F. H. Busse and H. Frick, Square-pattern convection in fluids with strongly temperature-dependent viscosity, *J. Fluid Mech.*, **150**, 451–465, (1975).

[12] D. A. Nield, The effect of temperature-dependent viscosity on the onset of convection in a saturated porous medium, *J. Heat Transfer*, **118**, 803–805, (1996).

[13] P. G. Siddheshwar, Thermorheological effect on magnetoconvection in weak electrically conducting fluids under $1g$ or μg, *Pramana*, **62**, 61–68, (2004).

[14] F. Pla and H. Herrero, Effects of non-uniform heating on a variable viscosity Rayleigh–Bénard problem, *Theor. Comput. Fluid Dyn.*, **25**, 301–313, (2011).

[15] E. Giannandrea and U. Christensen, Variable viscosity convection experiments with a stress-free upper boundary and implications for the heat transport in the Earth's mantle, *Phys. Earth Planet. Inter.*, **78**, 139–152, (1993).

[16] M. Tveitereid, Thermal convection in a horizontal porous layer with internal heat sources, *Int. J. Heat Mass Transf.*, **20**, 1045–1050, (1977).

[17] R. M. Clever, Heat transfer and stability properties of convection rolls in an internally heated fluid layer with an internal heat source, *J. Phys. Soc. Jpn.*, **53**, 4169–4178, (1977).

[18] N. Riahi, Nonlinear convection in a horizontal layer with an internal heat source, *J. Phys. Soc. Jpn.*, **S3**, 4169–4178, (1984).

[19] N. Riahi, Convection in a low Prandtl number fluid with internal heating, *Int. J. Non-Linear Mech.*, **21**, 97–107, (1986).

[20] P. G. Siddheshwar and P. Stephen Titus, Nonlinear Rayleigh-Bénard convection with variable heat source, *ASME J. Heat Transf.*, **135**, 122502, (2011).

[21] A. S. Aruna, Non-linear Rayleigh-Bénard magnetoconvection in temperature-sensitive Newtonian liquids with heat source, *Pramana*, **94**, 153, (2020).

[22] V. Ramachandramurthy and A. S. Aruna, Rayleigh-Bénard magnetoconvection in temperature-sensitive Newtonian liquids with heat source, *Math. Sci. Int. Res. J.*, **6**, 92–98, (2017).

[23] N. Kavitha, A. S. Aruna, M. S. Basavaraj and V. Ramachandramurthy, Non-linear Chandrasekhar-Bénard convection in temperature-dependent variable viscosity Boussinesq-Stokes suspension fluid with variable heat source/sink, *Appl. Math.*, (2022).

[24] V. Ramachandramurthy, A. S. Aruna and N. Kavitha, Bénard-Taylor convection in temperature-dependent variable viscosity Newtonian liquids with internal heat source, *Int. J. Appl. Comput. Math.*, **6**, 27, (2020).

[25] B. Y. Ogunmola, A. T. Akinshilo and M. G. Sobamowo, Perturbation solutions for Hagen-Poiseuille flow and heat transfer of third-grade fluid with temperature-dependent viscosity and internal heat generation, *Int. J. Eng. Math.*, 8915745, (2016).

[26] N. S. Lyutikas and A. A. Zhukauskas, An investigation of influence of variable viscosity on laminar heat transfer in a flat duct, *Int. Chem. Eng.*, **8**, 301, (1968).

[27] J. Severin and H. Herwig, Onset of convection in the Rayleigh-Bénard flow with temperature dependent viscosity: An asymptotic approach, *Z. Angew. Math. Phys.*, **50**, 375–386, (1999).

[28] P. G. Siddheshwar, V. Ramachandramurthy and D. Uma, Rayleigh–Bénard and Marangoni magnetoconvection in Newtonian liquid with thermorheological effects, *Int. J. Eng. Sci.*, **49**, 1078–1094, (2011).

[29] Y. H. Gangadharaiah and S. P. Suma, Effects of internal heat generation and variable viscosity on onset of Rayleigh-Benard convection, *Int. J. Comput. Technol.*, **5**, (2013).

[30] M. Arora, M. K. Sharma, Penetrative convection due to internal heating in a rotating magnetic nanofluid layer with variable gravity effect, Palest. J. Math., 14, 84–95,(2025).

[31] A. A. G. Aravind, J. Ravikumar, Heat transfer effects of thermal radiation on a nanofluid flow past an oscillating vertical plate with variable temperature in the presence of rotation, Palest. J. Math., 14, 427–436,(2025).

[32] V. Gosty, G. Srinivas, B. S. Babu, B. S. Goud, A. S. Hendy, M. M. Ali and M. R. Ali, Influence of variable viscosity and slip on heat and mass transfer of immiscible fluids in a vertical channel, *Case Stud. Therm. Eng.*, **58**, 104368, (2024).

[33] A. S. Aruna and N. Kavitha, Effect of noninertial acceleration on heat transfer by Rayleigh–Bénard magnetoconvection: Exploring nonlinear dynamics, *Heat Transfer*, **54**, 553–567, (2024).

[34] G. Amendola, M. Fabrizio, A. Manes, On energy stability for thermal convection in viscous fluids with memory, Palest. J. Math., 2, 144–158,(2013).

[35] A. T. Akinshilo, A. G. Davodi, H. Rezazadeh, G. Sobamowo, C. Tunç, Heat transfer and flow of MHD micropolar nanofluid through porous walls with magnetic field and thermal radiation, Palest. J. Math., 11(2), 604–616,(2022).

[36] M. Das, S. Nandi, B. Kumbhakar, Hall effect on unsteady MHD 3D Carreau nanofluid flow past a stretching sheet with Navier's slip and nonlinear thermal radiation, Palest. J. Math., 11, 95–108,(2022).

[37] J. K. Platten and J. C. Legros, *Convection in liquids*, Springer Science and Business Media, (2012).

Author information

A. S. Aruna, Department of Mathematics, Ramaiah Institute of Technology, Bangalore-560054, India.
E-mail: arunas@msrit.edu

Vijaya Kumar, Department of Mathematics, Ramaiah Institute of Technology, Bangalore-560054, India.
E-mail: vijayasowbhagya@gmail.com

K. R. Milana, Department of Mathematics, Ramaiah Institute of Technology, Bangalore-560054, India.
E-mail: milanakr111991@gmail.com

N. Kavitha, Department of Mathematics, Ramaiah Institute of Technology, Bangalore-56005, India.
E-mail: kavitha.n@msrit.edu

Received: 2025-09-04
Accepted: 2026-02-21